

Microstructure and 355 nm Laser-Induced Damage Characteristics of Al₂O₃ Films Irradiated with Oxygen Plasma under Different Energy

Dongping Zhang, Yan Li, Jingting Luo, Zhuanghao Zheng, Guangxing Liang,
Xingmin Cai, Fan Ye, Ping Fan, Jianjun Huang

Institute of Thin Film Physics and Applications, Shenzhen University, Shenzhen, China
Shenzhen Key Laboratory of Sensor Technology, Shenzhen, China
Email: zdpiom@163.com

Received February 21, 2013; revised March 22, 2013; accepted March 31, 2013

Copyright © 2013 Dongping Zhang *et al.* This is an open access article distributed under the Creative Commons Attribution License, which permits unrestricted use, distribution, and reproduction in any medium, provided the original work is properly cited.

ABSTRACT

Al₂O₃ films were prepared using electron beam evaporation at room temperature. The samples were irradiated with oxygen plasma under different energy. The variations in average surface defect density and root mean square (RMS) surface roughness were characterized using an optical microscope and an atomic force microscope. Surface average defect density increased after plasma treatment. The RMS surface roughness of the samples decreased from 1.92 nm to 1.26 nm because of surface atom restructuring after oxygen plasma conditioning. A 355 nm laser-induced damage experiment indicated that the as-grown sample with the lowest defect density exhibited a higher laser-induced damage threshold (1.12 J/cm²) than the other treated samples. Laser-induced damage images revealed that defect is one of the key factors that affect laser-induced damage on Al₂O₃ films.

Keywords: Thin Film; Laser-Induced Damage; Electron Beam Evaporation; Plasma Irradiation

1. Introduction

Alumina (Al₂O₃) films are among the widely used ultra-violet optical film materials because of their high thermal conductivity, good stability, and excellent optical transparency within a wide spectral range [1-4]. Al₂O₃ is used for the preparation of high-reflective mirrors, antireflective coatings, optical filters, and other laser mirrors for laser systems. In recent years, considerable attention has been given to Al₂O₃ thin films. Many techniques can be used to prepare Al₂O₃ films, such as reactive magnetron sputtering [5], molecular beam epitaxy [6], sol-gel [7], ion beam sputtering [8], chemical vapor deposition [9], atomic layer deposition [10], electron beam thermal evaporation [11], and so on. Among these techniques, electron beam evaporation is one of the most common methods for optical thin film deposition.

Optical coating mirrors are important but vulnerable components in laser systems [12,13]. Their susceptibility to laser-induced damage is one of the obstacles in the development of high-power laser technology. Many studies reported that micro-defects produced during the coating process caused by splashing and high absorption are

the two most critical factors that affect film laser damage threshold [14-16]. To improve the film laser damage threshold, many techniques were developed, such as reactive evaporation [17], laser conditioning [18], ion beam post-treatment [19], and so on. In this paper, Al₂O₃ films were deposited using electron beam evaporation, and the samples were irradiated with oxygen plasma under different energy densities. The microstructure and 355 nm laser-induced damage performance of the treated sample were studied.

2. Experiment Details

Al₂O₃ films were prepared on BK7 substrates at room temperature using electron beam thermal evaporation with a coating material purity of 99.99%. The base pressure in the vacuum chamber was 5.3×10^{-3} Pa. The coating material was pre-melted thoroughly before deposition until the pressure of the vacuum chamber stabilized. During deposition, the working pressure and electron beam current were maintained at 1.5×10^{-3} Pa and 200 mA, respectively. Film thickness, which was approximately 825 nm, was controlled using an optical

monitor. Oxygen gas with a purity of 99.99% was ionized by an ion source to produce oxygen plasma. The prepared film samples were irradiated with oxygen plasma under different energy densities. The distance from the ion source to the sample surface was approximately 0.5 m. The angle between the ion beam and the normal direction of the sample surface was approximately 60° . The detailed ion source parameters are shown in **Table 1**. During the treatment process, the oxygen gas flow rate was 8 sccm, the pressure of the vacuum chamber was 0.1 Pa, and the ion beam current was 10 mA. The treatment time was 10 min. The applied ion energy varied from 350 eV to 500 eV for the different samples (**Table 2**).

The micro-defect density of the sample surface was determined using a Leica DM4000 microscope in dark field mode. The statistical criterion was the observation of visible defect under $200\times$ magnification. The microstructure of the sample surface before and after the treatment was examined using an atomic force microscope (AFM). The samples were scanned over a $1\ \mu\text{m} \times 1\ \mu\text{m}$ area using the contacting mode. The image resolution was 256×256 pixels. The laser-induced damage threshold (LIDT) of the samples was tested according to the ISO11254-1-2000 standard in 1-on-1 mode [20]. A Q-switched Nd: YAG single-mode laser with an 8 ns pulse width and a 355 nm wavelength was used. The laser spot area on the sample surface measured using the knife-edge scanning method [21] was $0.026\ \text{mm}^2$. Laser was irradiated in the direction of normal incidence of the sample surface. The testing system could see in our previous research work [22]. Laser-induced damage morphologies were characterized and analyzed under a Leica polarizing microscope.

3. Results and Analysis

Eight sites were randomly selected on each sample surface to measure the average defect density. The relationship between the oxygen plasma energy and average defect density is shown in **Figure 1**. The plot shows that defect density increased in different degrees after irradiation with oxygen plasma.

Table 1. Parameters of the ion source.

Screen voltage (kV)	Acceleration voltage (V)	Cathode voltage (V)	Anode voltage (V)	Ion beam current (mA)
0.506	230	14	70 - 75	10

Table 2. Plasma energy for samples treatment.

Sample ID	A0 (as-grown)	A1	A2	A3	A4
Plasma energy (eV)	-	350	400	450	500

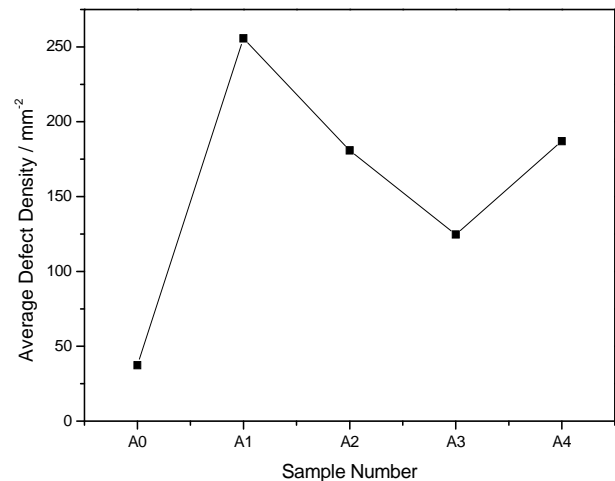


Figure 1. Average defect density of samples surface irradiated with different energy of oxygen plasma.

Considering the plasma treatment process, we can deduce that the increase in defect density may be related to the second contaminant in the pumping and plasma treatment process. Compared with that of the as-grown sample, the average defect density of the Al_2O_3 film increased greatly after irradiation with lower plasma energy at the initial stage. This phenomenon may be attributed to the limited ability of the low-energy oxygen plasma irradiation to remove a small amount of contaminant. As the plasma energy increased, more particle defects were partially removed, and the defect density reduced. When the plasma energy was too high, fresh defects will be produced from the berried defects, thereby increasing defect density.

The AFM images of the samples are shown in **Figure 2**. The relationship between the root mean square (RMS) surface roughness of the sample and the oxygen plasma energy is plotted in **Figure 3**. Rough structure can be clearly observed from the as-grown sample surface image. The sample RMS roughness decreased as the oxygen plasma energy increased. The RMS roughness of the samples decreased from 1.92 nm to 1.26 nm when plasma energy varied from 0 eV (as-grown sample) to 500 eV. In most cases, many surface atoms reside in metastable state. During the oxygen plasma irradiation process, these atoms are relocated to the surface and transformed from metastable to stable state after gaining sufficient energy. The surface microstructure is restructured, and the surface RMS roughness is reduced correspondingly [23].

Figure 4 shows the third harmonic LIDT fitting plots of the as-grown and treated samples at 355 nm. The largest slope of the fitting line of the as-grown sample compared with the irradiated samples can be observed. This result reveals that the laser damage characteristics of the as-grown sample determine the intrinsic properties of thin-film materials [24]. However, damage on the

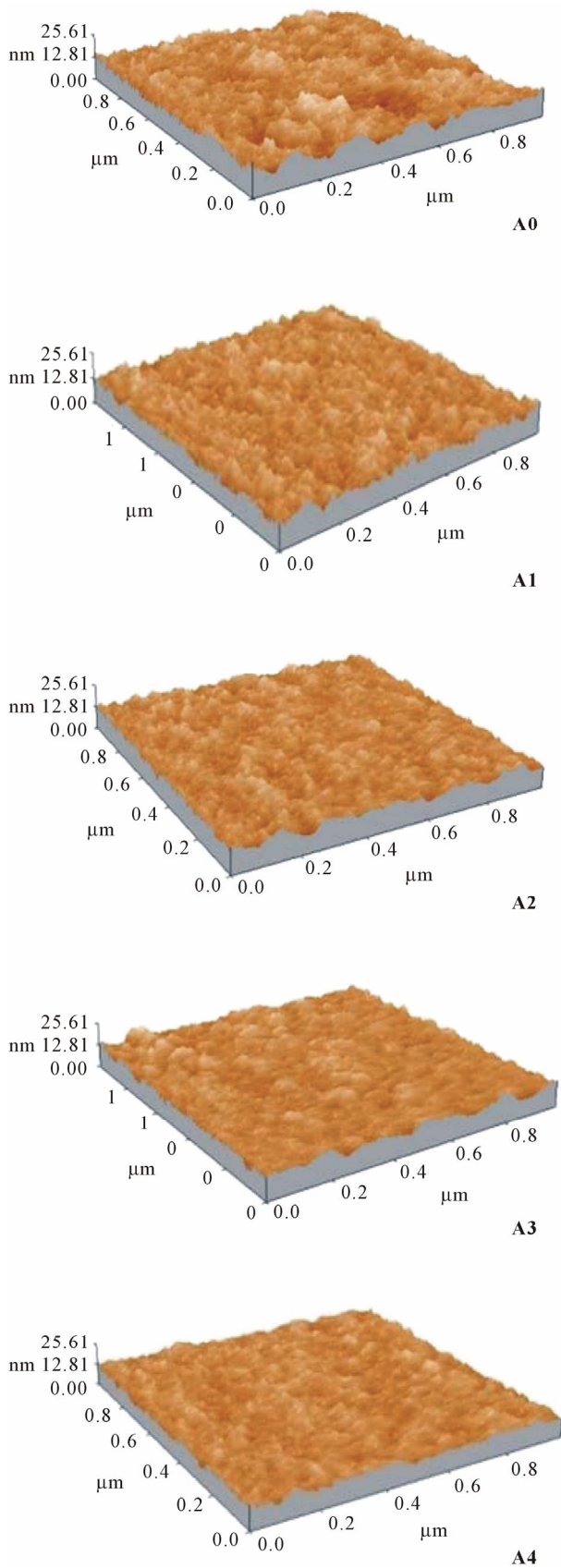


Figure 2. AFM images of the samples.

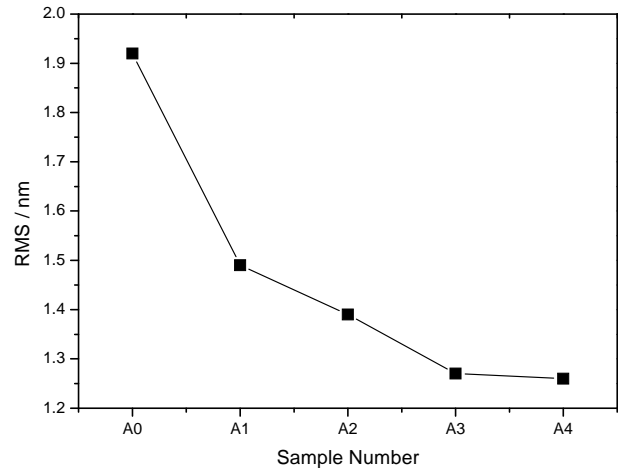


Figure 3. RMS roughness variations of the samples.

treated samples presents a semblance of defect-induced failure characteristics. **Figure 5** shows the LIDT variations in the samples at 355 nm. The LIDT of the samples varied from 1.12 J/cm^2 to 0.82 J/cm^2 . The highest LIDT of the as-grown sample is revealed from the plots. A comparison of the defect density measurement results in **Figure 1** with the lowest defect density of the as-grown sample shows that the highest LIDT observed is reasonable.

Laser-damage morphologies of the films after irradiation with various energy densities are shown in **Figure 6**. The damage scars are in micrometer size. Given the energy density Gaussian distribution of the laser beam, a catastrophic damage in the scar center can be observed. Moreover, the damage mostly occurred and developed from the defect sites, which correspond to the LIDT measurement results in **Figure 5**. At low energy density, numerous pustules developed because of the increase in defects after laser energy absorption (**Figure 6(a)**). As the laser energy increased, the pustules cracked and damage pits were produced (**Figure 6(b)**). When laser energy density further increased, damage on the entire spot area occurred (**Figure 6(c)**).

4. Conclusion

Al_2O_3 thin films were prepared using electron beam evaporation. The samples were irradiated with oxygen plasma under different energy densities. Surface average defect density increased after plasma treatment. The RMS surface roughness of the samples decreased because of surface atom restructuring after oxygen plasma conditioning. The as-grown sample with the lowest defect density exhibited a higher 355 nm LIDT (1.12 J/cm^2) than the other samples. Laser-induced damage images revealed that defect is one of the key factors that affect laser-induced damage on Al_2O_3 films. Thus, defect density reduction should be monitored during Al_2O_3 film production.

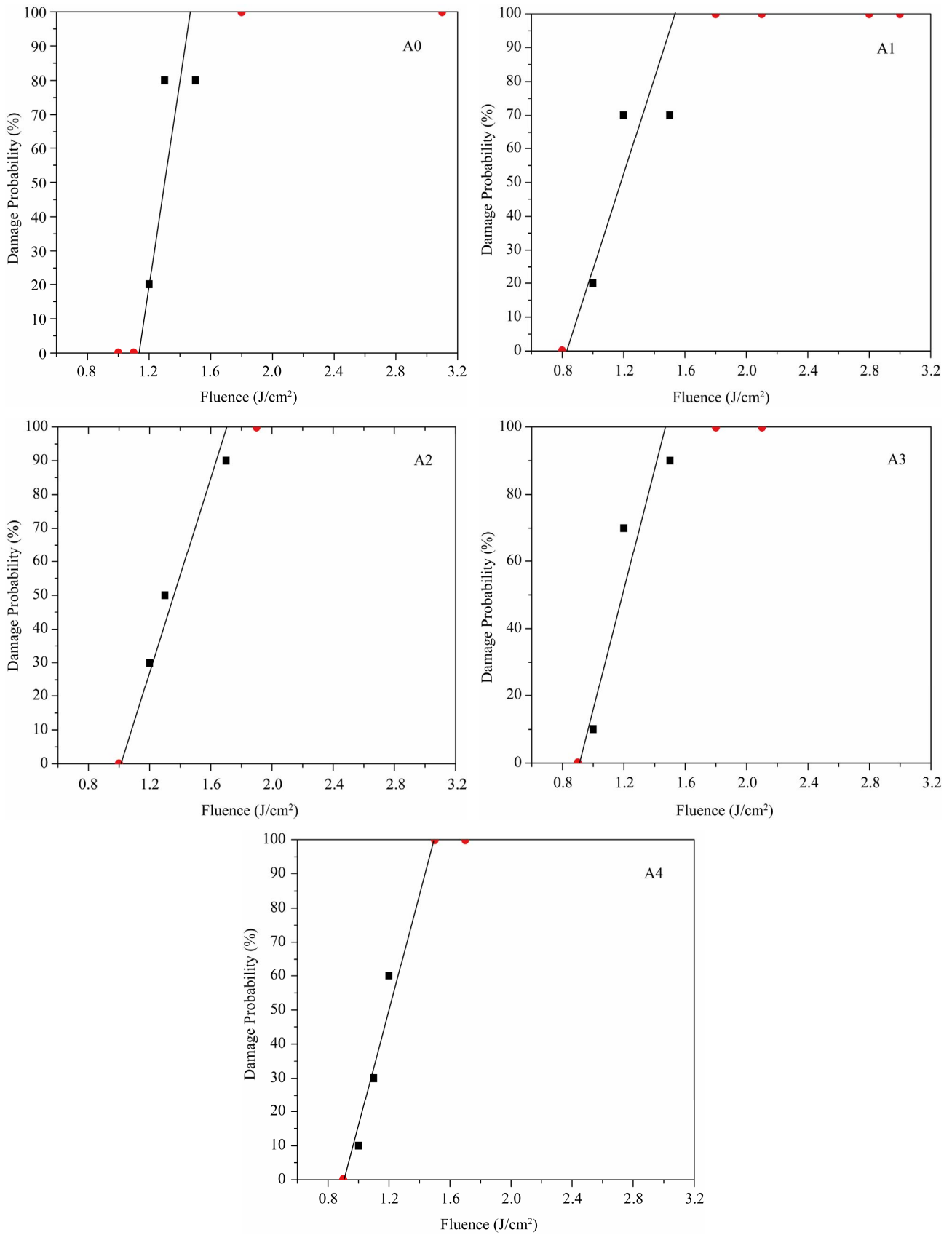


Figure 4. Laser induced damage threshold fitting lines of samples.

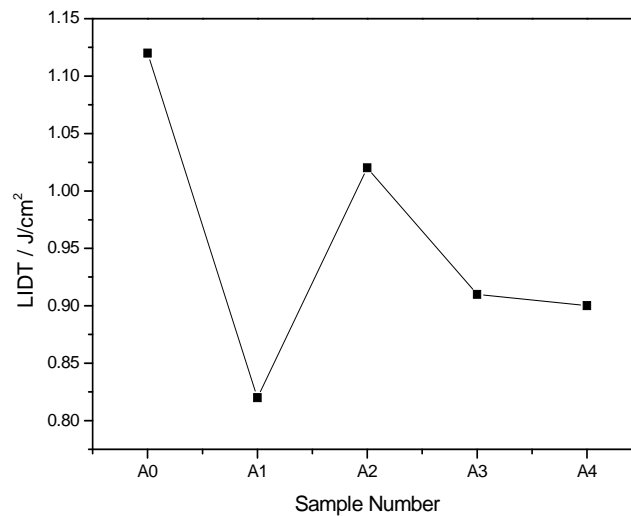


Figure 5. Laser-induced damage threshold variation of the as-grown and treated samples.

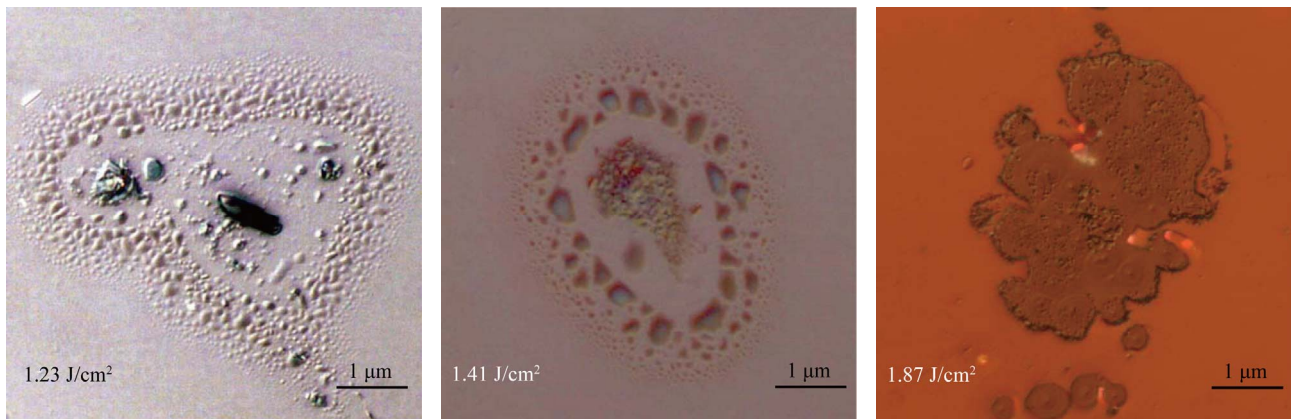


Figure 6. Microscope images of the laser-induced damage morphology of samples.

5. Acknowledgements

The work was supported by National Natural Science Foundation of China (Grant. No. 11174208) and Basic Research Project of Shenzhen Government (Grant. No. GJHS20120621155804681). Authors also to thank Dr. Dawei Li and Wenwen Liu for their help of laser damage testing.

REFERENCES

- [1] B. Cho, J. E. Rudisill and E. Danielewicz, "193 nm Laser Induced Spectral Shift in HR Coated Mirrors," *Optical Engineering*, Vol. 51, No. 12, 2012, Article ID: 121804. [doi:10.1117/1.OE.51.12.121804](https://doi.org/10.1117/1.OE.51.12.121804)
- [2] R. Thielsch, A. Gatto, J. Heber and N. Kaiser, "A Comparative Study of the UV Optical and Structural Properties of SiO₂, Al₂O₃, and HfO₂ Single Layers Deposited by Reactive Evaporation, Ion-Assisted Deposition and Plasma Ion-Assisted Deposition," *Thin Solid Films*, Vol. 410, No. 1-2, 2002, pp. 86-93. [doi:10.1016/S0040-6090\(02\)00208-0](https://doi.org/10.1016/S0040-6090(02)00208-0)
- [3] M. Reichling A. Bodemann and N. Kaiser, "Defect Induced Laser Damage in Oxide Multilayer Coatings for 248 nm," *Thin Solid Films*, Vol. 320, No. 2, 1998, pp. 264-279. [doi:10.1016/S0040-6090\(97\)00399-4](https://doi.org/10.1016/S0040-6090(97)00399-4)
- [4] J. Koo, S. Kim, S. Jeon, H. Jeon, Y. Kim and Y. Won, "Characteristics of Al₂O₃ Thin Films Deposited Using Dimethylaluminum Isopropoxide and Rimethylaluminum Precursors by the Plasma-Enhanced Atomic-Layer Deposition Method," *Journal of the Korean Physical Society*, Vol. 48, No. 1, 2006, pp. 131-136.
- [5] X. Tang, F. Luo, W. Zhou and D. Zhu, "Alumina Thin Film Prepared by Direct Current Reactive Magnetron Sputtering," *Hot Working Technology*, Vol. 40, No. 14, 2011, pp. 120-123.
- [6] V. V. Mamutin, V. A. Vekshin, V. Y. Davydov, V. V. Ratnikov, Y. A. Kudriavtsev, B. Y. Ber, V. V. Emtsev and S. V. Ivanov, "Mg-Doped Hexagonal InN/Al₂O₃ Films Grown by MBE," *Physica Status Solidi A—Applied Research*, Vol. 176, No. 1, 1999, pp. 373-378. [doi:10.1002/\(SICI\)1521-396X\(199911\)176:1<373::AID-PSSA373>3.0.CO;2-1](https://doi.org/10.1002/(SICI)1521-396X(199911)176:1<373::AID-PSSA373>3.0.CO;2-1)
- [7] T. Ivanova, A. Harizanova, T. Koutzarova and B. Ver-

- truyen, "Preparation and Characterisation of Ag Incorporated Al_2O_3 Nanocomposite Films Obtained by Sol-Gel Method," *Crystal Research and Technology*, Vol. 47, No. 5, 2012, pp. 579-584. [doi:10.1002/crat.201200027](https://doi.org/10.1002/crat.201200027)
- [8] N. Matsumura and T. Hayashi, "Preparation of Crystalline Al_2O_3 Films by Ion Beam Sputtering Combined with Oxygen Ion Irradiation and Their Wear Resistance Properties," *Journal of the Japan Institute of Metals*, Vol. 61, No. 6, 1997, pp. 528-534.
- [9] X. Duan, N. H. Tran, N. K. Roberts and R. N. Lamb, "Single-Source Chemical Vapor Deposition of Clean Oriented Al_2O_3 Thin Films," *Thin Solid Films*, Vol. 517, No. 24, 2009, pp. 6726-6730. [doi:10.1016/j.tsf.2009.05.032](https://doi.org/10.1016/j.tsf.2009.05.032)
- [10] K. S. Shamala, L. C. S. Murthy and K. Narasimha Rao, "Studies on Optical and Dielectric Properties of Al_2O_3 Thin Films Prepared by Electron Beam Evaporation and Spray Pyrolysis Method," *Materials Science and Engineering B*, Vol. 106, No. 3, 2004, pp. 269-274. [doi:10.1016/j.mseb.2003.09.036](https://doi.org/10.1016/j.mseb.2003.09.036)
- [11] M.-Q. Zhan, Z.-L. Wu and Z.-X. Fan, "Working Pressure Dependence of Properties of Al_2O_3 Thin Films Prepared by Electron Beam Evaporation," *Chinese Physics Letters*, Vol. 25, No. 2, 2008, p. 563. [doi:10.1088/0256-307X/25/2/057](https://doi.org/10.1088/0256-307X/25/2/057)
- [12] S. L. Chen, Y. A. Zhao, Z. K. Yu, Z. Fang, D. W. Li, H. B. He and J. D. Shao, "Femtosecond Laser-Induced Damage of $\text{HfO}_2/\text{SiO}_2$ Mirror with Different Stack Structure," *Applied Optics*, Vol. 51, No. 25, 2012, pp. 6188-6195. [doi:10.1364/AO.51.006188](https://doi.org/10.1364/AO.51.006188)
- [13] M. Zhou, J. D. Shao, Z. X. Fan, Y. A. Zhao and D. W. Li, "Effect of Multiple Wavelengths Combination on Laser-Induced Damage in Multilayer Mirrors," *Optics Express*, Vol. 17, No. 22, 2009, pp. 20313-20320. [doi:10.1364/OE.17.020313](https://doi.org/10.1364/OE.17.020313)
- [14] Z. L. Xia, R. Wu and H. Wang, "Laser Damage Mechanism of Porous Al_2O_3 Films Prepared by a Two-Step Anodization Method," *Optics Communications*, Vol. 285, No. 6, 2012, pp. 1335-1340. [doi:10.1016/j.optcom.2011.10.059](https://doi.org/10.1016/j.optcom.2011.10.059)
- [15] B. Wang, Y. Qin, X. W. Ni, Z. H. Shen and J. Lu, "Effect of Defects on Long-Pulse Laser-Induced Damage of Two Kinds of Optical Thin Films," *Applied Optics*, Vol. 49, No. 29, 2010, pp. 5537-5544. [doi:10.1364/AO.49.005537](https://doi.org/10.1364/AO.49.005537)
- [16] J. Dijon, T. Poiroux and C. Desrumaux, "Nano Absorbing Centers: A Key Point in Laser Damage of Thin Films," *SPIE Proceedings*, Vol. 2966, 1997, pp. 315-325. [doi:10.1117/12.274229](https://doi.org/10.1117/12.274229)
- [17] D. Reicher, P. Black and K. Jungling, "Defect Formation in Hafnium Dioxide Thin Films," *Applied Optics*, Vol. 39, No. 10, 2000, pp. 1589-1599. [doi:10.1364/AO.39.001589](https://doi.org/10.1364/AO.39.001589)
- [18] X. Li, X. F. Liu, Y. A. Zhao, J. D. Shao and Z. X. Fan, "Laser-Conditioning Mechanism of $\text{ZrO}_2/\text{SiO}_2$ HR Films with Fitting Damage Probability Curves of Laser-Induced Damage," *Chinese Optics Letters*, Vol. 8, No. 6, 2010, pp. 598-600. [doi:10.3788/COL20100806.0598](https://doi.org/10.3788/COL20100806.0598)
- [19] D. P. Zhang, J. D. Shao, D. W. Zhang, S. H. Fan, T. Y. Tan and Z. X. Fan, "Employing Oxygen-Plasma Posttreatment to Improve the Laser-Induced Damage Threshold of ZrO_2 Films Prepared by the Electron Beam Evaporation Method," *Optics Letters*, Vol. 29, No. 24, 2004, pp. 2870-2872. [doi:10.1364/OL.29.002870](https://doi.org/10.1364/OL.29.002870)
- [20] ISO 11254-1:2000, "Lasers and Laser Related Equipment Determination of Laser-Induced Damage Threshold of Optical Surfaces," Part I. 1-on-1 Test.
- [21] M. A. C. de Araújo, R. Silva, E. de Lima, D. P. Pereira and P. C. de Oliveira, "Measurement of Gaussian Laser Beam Radius Using the Knife-Edge Technique: Improvement on Data Analysis," *Applied Optics*, Vol. 48, No. 2, 2009, pp. 393-396. [doi:10.1364/AO.48.000393](https://doi.org/10.1364/AO.48.000393)
- [22] D. P. Zhang, J. D. Shao, Y. A. Zhao, S. H. Fan, R. J. Hong and Z. X. Fan, "Laser-Induced Damage Threshold of ZrO_2 Thin Films Prepared at Different Oxygen Partial Pressures by Electron-Beam Evaporation," *Journal of Vacuum Science & Technology A*, Vol. 23, 2005, pp. 197-200. [doi:10.1116/1.1842111](https://doi.org/10.1116/1.1842111)
- [23] D. P. Zhang, P. Fan, X. M. Cai, G. X. Liang and J. D. Shao, "Influence of Oxygen Plasma Treatment on Properties of ZrO_2 Films Prepared by e-Beam Evaporation Techniques," *Solid State Communications*, Vol. 148, No. 1-2, 2008, pp. 22-24. [doi:10.1016/j.ssc.2008.07.019](https://doi.org/10.1016/j.ssc.2008.07.019)
- [24] C. Xu, S. Yang, S. H. Zhang, J. N. Niu, Y. H. Qiang, J. T. Liu and D. W. Li, "Temperature Dependences of Optical Properties, Chemical Composition, Structure, and Laser Damage in Ta_2O_5 Films," *Chinese Physics B*, Vol. 21, No. 11, 2012, Article ID: 114213. [doi:10.1088/1674-1056/21/11/114213](https://doi.org/10.1088/1674-1056/21/11/114213)